Inorg. Chem. **2005**, *44*, 9643–9651

Metal–Metal Bond or Isolated Metal Centers? Interaction of $Hg(CN)_2$ with Square Planar Transition Metal Cyanides

Róbert Jószai,[†] Imre Beszeda,[‡] Attila C. Bényei,[§] Andreas Fischer,[£] Margit Kovács,[||] Mikhail Maliarik,[#] Péter Nagy,[†] Andrey Shchukarev,[+] and Imre Tóth*,[†]

Department of Inorganic and Analytical Chemistry, University of Debrecen, H-4010 Debrecen Pf. 21, Hungary, Department of Solid State Physics, University of Debrecen, H-4010 Debrecen, Pf. 2, Hungary, Department of Chemistry, University of Debrecen, H-4010 Debrecen, Pf. 7, Hungary, Department of Chemistry, Inorganic Chemistry, The Royal Institute of Technology (KTH), S-100 44 Stockholm, Sweden, Department of General and Inorganic Chemistry, University of Veszprém, H-8201 Veszprém, Pf. 158., Hungary, IFM-Department of Chemistry, Linköping University, S-581 83 Linköping, Sweden, and Department of Chemistry, Inorganic Chemistry, Umeå University, SE−901 87 Umeå, Sweden

Received March 7, 2005

Three adducts have been prepared from $Hg(CN)_2$ and square planar $M^{II}(CN)_4^{2-}$ transition metal cyanides (M = Pt, Pd, or Ni, with d^8 electron shell) as solids. The structure of the compounds $K_2PtHg(CN)_6 \cdot 2H_2O$ (**1**), $Na_2PdHg(CN)_6 \cdot 2H_2O$ (**2**), and $K_2NiHg(CN)_6 \cdot 2H_2O$ (**3**) have been studied by single-crystal X-ray diffraction, XPS, Raman spectroscopy, and luminescence spectroscopy in the solid state. The structure of $K_2PtHg(CN)_6 \cdot 2H_2O$ consists of one-dimensional wires. No CN^- bridges occur between the heterometallic centers. The wires are strictly linear, and the Pt(II) and Hg(II) centers alternate. The distance d_{Hg-Pt} is relatively short, 3.460 Å. Time-resolved luminescence spectra indicate that $Hg(CN)_2$ units incorporated into the structure act as electron traps and shorten the lifetime of both the short-lived and longer-lived exited states in **1** compared to $K_2[Pt(CN)_4] \cdot 2H_2O$. The structures of $Na_2PdHg(CN)_6 \cdot 2H_2O$ and $K_2NiHg(CN)_6 \cdot 2H_2O$ can be considered as double salts; the lack of heterometallophilic interaction between the remote Hg(II) and Pd(II) atoms, d_{Hg-Pd} = 4.92 Å, and Hg(II) and Ni(II) atoms, d_{Hg-Ni} = 4.61 Å, is apparent. Electron binding energy values of the metallic centers measured by XPS show that there is no electron transfer between the metal ions in the three adducts. In solution, experimental findings clearly indicate the lack of metal–metal bond formation in all studied Hg^{II}–CN^-–$M^{II}(CN)_4^{2-}$ systems (M = Pt, Pd, or Ni).

Introduction

Recently, the metallophilic interactions between heavy elements[1] have earned considerable interest. Metal cyanides are known to form hetero-dimetallic complexes.[2] Our contribution to this subject is the discovery of a new family of platinum−thallium complexes. The formation,[3] structure,[4−6] equilibrium,[7] and kinetics of formation[8,9] of a family of cyano compounds containing a direct (but not supported by ligands) platinum−thallium metal−metal bond have been reported. The compounds are diamagnetic, and the electronic states and the nature of the Pt−Tl bonds have been elucidated by DFT calculation.[10]

One of the earliest detailed descriptions[11] of a luminescent compound in the literature is that of the $K_2[Pt(CN)_4]$. The

* To whom correspondence should be addressed. E-mail: imretoth@delfin.klte.hu.
[†] Department of Inorganic and Analytical Chemistry, University of Debrecen.
[‡] Department of Solid State Physics, University of Debrecen.
[§] Department of Chemistry, University of Debrecen.
[£] The Royal Insititute of Technology.
[||] University of Veszprém.
[#] Linköping University.
[+] Umeå University.

(1) Pyykkö, P. *Chem. Rev.* **1997**, *97*, 597−636.
(2) Beck, M. T.; Porzsolt, É. C. *J. Coord. Chem.* **1971**, *1*, 57−66.
(3) Maliarik, M.; Berg, K.; Glaser, J.; Sandström, M.; Tóth, I. *Inorg. Chem.* **1998**, *37*, 2910−2919.
(4) Jalilehvand, F.; Maliarik, M.; Sandström, M.; Mink, J.; Persson, I.; Persson, P.; Tóth, I.; Glaser, J. *Inorg. Chem.* **2001**, *40*, 3889−3899.
(5) Jalilehvand, F.; Eriksson, L.; Glaser, J.; Maliarik, M.; Mink, J.; Sandström, M.; Tóth, I.; Tóth, J. *Chem. Eur. J.* **2001**, *7*, 2167−2177.
(6) Ma, G.; Kritikos, M.; Maliarik, M.; Glaser, J. *Inorg. Chem.* **2004**, *43*, 4328−4340.
(7) Maliarik, M.; Glaser, J.; Tóth, I.; W. da Silva, M.; Zékány, L. *Eur. J. Inorg. Chem.* **1998**, 565−570.
(8) Nagy, P.; Tóth, I.; Fábián, I.; Maliarik, M.; Glaser, J. *Inorg. Chem.* **2003**, *42*, 6907−6914.
(9) Nagy, P.; Tóth, I.; Fábián, I.; Maliarik, M.; Glaser, J. *Inorg. Chem.* **2004**, *43*, 5216−5221.

10.1021/ic050352c CCC: $30.25
Published on Web 11/17/2005

optical properties of crystalline $[Pt(CN)_4]^{2-}$ compounds of columnar structure and those of $[Pt(CN)_4]^{2-}$ oligomers formed in solution at high solute concentration have been proved to be mainly determined by the Pt−Pt distances (depending on several other parameters, e.g., temperature, pressure, concentration, external electric, and magnetic field).[12−15] The photoexcitation of crystals results in typical double-exponential emission, assigned as the transition from the higher-energy, delocalized, exciton-state and a radiative decay of the lower-energy, self-trapped, exciton state.

To obtain a deeper insight into the nature of the interaction between Pt(II) with d^8 and the Tl(III) with $d^{10}s^0$ electronic structures, a study of $[Pt(CN)_4]^{2-}$ with Hg(II) being isoelectronic with Tl(III) has been carried out in aqueous solution and in the solid phase. The crystal structure of the $K_2PtHg(CN)_6 \cdot 2H_2O$ adduct (first mentioned in the literature 86 years ago by Strömholm[16]) has been solved. Investigation of the systems consisting of the lighter analogues of Pt(II), namely the $[Pd(CN)_4]^{2-}$ and $[Ni(CN)_4]^{2-}$ with $Hg(CN)_2$, have also been made and reported here.

Experimental Section

1. Materials. $K_2[Pt(CN)_4] \cdot 3H_2O$, $K_2[PdCl_4]$ (Aldrich, reagent grade), $NiSO_4 \cdot 7H_2O$, NaCN, KCN, and $Hg(CN)_2$ (Reanal, reagent grade) came from commercial sources.

1.1. $Na_2[Pd(CN)_4] \cdot 3H_2O$. The salt was obtained by an exchange reaction between $K_2[PdCl_4]$ and NaCN in aqueous solution with a molar ratio CN/Pd of 6, followed by a recrystallization of the tetracyano-palladate salt. Anal. Calcd (%) for $Na_2[Pd(CN)_4] \cdot 3H_2O$: Pd 34.3; Na 14.8. Found: Pd 33.9; Na 14.4.

1.2. $K_2[Ni(CN)_4] \cdot 3H_2O$. $NiSO_4 \cdot 7H_2O$ (7.5 g, 26.5 mmol) was dissolved in 25 cm^3 of water at 60 °C and 3.5 g of NaCN (53 mmol, dissolved in 10 cm^3 of water) was added to the solution while stirring. Pale blue $Ni(CN)_2$ was formed, and the slurry was kept at 60 °C for 10 min. It was separated by a centrifuge and washed with water. The freshly prepared $Ni(CN)_2$ was dissolved in 6 cm^3 of an aqueous solution containing 3.5 g of NaCN (53 mmol). The red solution was concentrated in a steam bath until precipitation started, and then it was cooled to room temperature. The orange-colored crystals were filtered, washed by cold water, and dried in air. Yield: 2.57 g (33%).

2. Preparation of Heterometallic Adducts. 2.1. $K_2PtHg(CN)_6 \cdot 2H_2O$ (1). $K_2[Pt(CN)_4] \cdot 3H_2O$ (100 mg, 0.23 mmol) and 58 mg (0.23 mmol) of $Hg(CN)_2$ were dissolved in 0.23 cm^3 of distilled water at 80 °C ($c_{Pt} = c_{Hg} = 1$ M) in a small screw-cap vessel. The vessel was allowed to cool slowly to room temperature. The crystals were filtered by a G3 filter, kept in air until constant weight, and measured. Yield: 95 mg (65%). The molar ratio of K/Pt/Hg = 2:1:1 was measured by a scanning electron microscope.

2.2. $Na_2PdHg(CN)_6 \cdot 2H_2O$ (2). $Na_2[Pd(CN)_4] \cdot 3H_2O$ (31 mg, 0.1 mmol) and 25 mg (0.1 mmol) of $Hg(CN)_2$ were dissolved in 0.20 cm^3 of distilled water at 25 °C ($c_{Pd} = c_{Hg} = 0.5$ M) in a small vessel. Slow evaporation of the solvent resulted in colorless $Na_2PdHg(CN)_6 \cdot 2H_2O$ crystals.

2.3. $K_2NiHg(CN)_6 \cdot 2H_2O$ (3). 3 was prepared in a similar manner as in the case of **1** but 1.25 mmol of both $K_2[Ni(CN)_4] \cdot 3H_2O$ and $Hg(CN)_2$ were dissolved in 2.5 cm^3 ($c_{Ni} = c_{Hg} = 0.5$ M) of distilled water. Yield: 0.41 g (60%).

Selected crystals (**1**, as well as **2** and **3**) were used for X-ray study. Powder samples, made in identical preparations, were used for Raman spectroscopy, X-ray photoelectron spectroscopy (XPS), and luminescence spectroscopy.

3. Analysis. The atomic ratio of the adducts was checked by XPS and/or by an AMRAY 1830I Scanning Electron Microscope. The estimated uncertainties are ±10% rel in atomic ratios.

3.1. UV−Vis. UV−vis spectrophotometric measurements were made with a CARY 1E UV−visible spectrophotometer using a Hellma QS cuvette with 0.01 mm path length.

3.2. NMR. ^{13}C NMR spectra were recorded by a Bruker AM 360 instrument: SF = 80 MHz, PW= 10 μs (30°), delay between pulses AQ + RD= 10 s. Chemical shifts refer to TMS* as external standard. ^{195}Pt NMR measurements were carried out by a Bruker DRX 500, typical parameters were SF = 96.7 MHz, PW = 10 μs (30°), AQ + RD = 2 s, 2000 scans. Chemical shift is referred to $Na_2[PtCl_6]$ as external standard, $\delta = 4533$ ppm to higher frequency from Ξ (^{195}Pt) = 21.4 MHz at 25 °C.

3.3. Raman Spectroscopy. Raman spectra of the crystalline samples were measured by using a Renishaw System 1000 spectrometer, equipped with a Leica DMLM microscope, a 25 mW diode laser (780 nm), and a Peltier-cooled CCD detector.

3.4. Single-Crystal X-Ray. X-ray-quality crystals were fixed onto the tip of a glass fiber with epoxy glue. Data for **1** and **3** were collected at 293(1) K, using a Enraf Nonius MACH3 diffractometer, Mo Kα radiation, $\lambda = 0.71073$ Å, $\omega-2\theta$ motion. The structure was solved using heavy-atom methods and refined on F^2 using the SHELX-97 program.[17] Publication material was prepared with WINGX-97.[18] Other details of X-ray structure determination are summarized in Table 1. Only a fraction of very high angle ($\theta > 25°$) reflections were collected. Residual electron density peaks were close to heavy atoms. Empirical absorption correction was made[19] using the ψ scan method. The data for **2** were collected on a Bruker−Nonius KappaCCD diffractometer at 299 K using Mo Kα radiation, $\lambda = 0.71073$ Å. All crystals of **2** turned out to be twinned. Orientation matrixes for both twin domains were obtained using Dirax.[20] During the integration, all overlapping reflections were omitted using EvalCCD.[21] The structure was solved using direct methods and refined on F^2.[17] The oxygen atom turned out to be disordered. By applying split positions, the quality of the structural model could be improved.

3.5. XPS Measurements. All XPS spectra were recorded with a Kratos Axis Ultra electron spectrometer using a monochromatic Al K_α source operated at 180 W and with a charge neutralizer. To avoid loss of water and minimize possible X-ray degradation of samples, a liquid nitrogen precooling procedure was carried out before the measurements. This procedure includes (a) precooling the end of the sample transfer rod (20 min at −170 °C), (b) sample loading and waiting 30 s, and (c) pumping of the introducing

(10) Autschbach, J.; Ziegler, T. *J. Am. Chem. Soc.* **2001**, *312*, 221.
(11) Khvostikov, J. A. *Tr. Gos. Optich. Inst. Leningrad* **1937**, *12*, 8−11.
(12) Gliemann, G.; Otto, H.; Yersin, H. *Chem. Phys. Lett.* **1975**, *36*, 86−87.
(13) Stock, M.; Yersin, H. *Chem. Phys. Lett.* **1976**, *40*, 423−428.
(14) Schindler, J. W.; Fukuda, R. C.; Adamson, A. W. *J. Am. Chem. Soc.* **1982**, *104*, 3596−3600.
(15) Hidvegi, I.; von Ammon; Gliemann, G. J. *J. Phis. Chem.* **1982**, *76*, 4361−4369.
(16) Strömholm, Z. *Anorg. Chem.* **1919**, *108*, 1.
(17) Sheldrick, G. M. *SHELXS*97 *and SHELXL*97; University of Göttingen: Göttingen, Germany, 1997.
(18) Farrugia, L. J. *WINGX-97 system*; University of Glasgow: Glasgow, UK, 1996.
(19) North, A. C. T.; Phillips, D. C.; Mathews, F. S. *Acta Crystallogr.* **1968**, *A24*, 351−359.
(20) Duisenberg, A. J. M. *J. Appl. Crystallogr.* **1992**, *25*, 92−96.
(21) Duisenberg, A. J. M.; Kroon-Batenburg, L. M. J.; A. M. M. Schreurs, J. *J. Appl. Crystallogr.* 2003, *36*, 220−229.

Table 1. Crystal Data and Structure Refinement for **1**, **2**, and **3**

empirical formula	$C_6H_4HgK_2N_6O_2Pt$ (**1**)	$C_6H_4HgNa_2N_6O_2Pd$ (**2**)	$C_6H_4HgK_2N_6NiO_2$ (**3**)
fw	666.03	541.076	529.65
temp (K)	293	299	293
wavelength (Å)	0.71073	0.71073	0.71073
cryst syst	monoclinic	triclinic	monoclinic
space group	*P*21/*c* (No. 14)	$P\bar{1}$	*C*2/*c* (No. 15)
unit cell dimensions			
a (Å)	9.9880(10)	3.770(2)	18.9710(30)
b (Å)	6.9208(10)	9.172(4)	4.0243(10)
c (Å)	11.2143(10)	9.838(4)	18.240(3)
α(°)		102.94(3)	
β(°)	113.00(1)	100.88(2)	94.13(2)
γ(°)		94.85(4)	
V (Å^3)	713.5(1)	322.7(2)	1388.9(5)
Z	2	2	4
D_{calc} (Mg m^{-3})	3.1	2.784	2.533
absorption coefficient (mm^{-1})	21.12	13.3	13
F (000)	588	242	976
cryst size (mm^3)	0.5 × 0.1 × 0.06	0.12 × 0.06 × 0.06	0.54 × 0.2 × 0.15
cryst color	colorless	colorless	colorless
habit	needle	needle	rod
θ range for data collection	2.46−29.9	5.52−27.49	2.2−25.29
index ranges	$-1 \le h \le 7$	$-4 \le h \le 4$	$0 \le h \le 22$
	$-2 \le k \le 8$	$-11 \le k \le 11$	$0 \le k \le 4$
	$-13 \le l \le 13$	$-12 \le l \le 12$	$-21 \le l \le 21$
reflns collected	1594	4181	1743
independent reflns	1594 [$R_{int} = 0.0104$]	1245 [$R_{int} = 0.053$]	1263 [$R_{int} = 0.06$]
completeness of data	67%	84%	99.90%
absorption correction	empirical (*ψ* scan)	numerical	empirical (*ψ* scan)
max/min transmission	0.0226/ 0.777	0.30/0.43	0.012/0.0524
decay (%)	none	none	1
refinement method		full matrix least-squares on F^2	
data/restraints/params	1594/0/92	1245/0/94	1743 /0/85
final *R* indices [all data]	R1 = 0.0224, wR2 = 0.0935	R1 = 0.0265, wR2 = 0.0498	R1 = 0.0515, wR2 = 0.176
GOF on F^2	0.695	1.124	1.186
largest difference peak and hole	0.575/−0.927 (e Å^{-3})	0.72/−0.90 (e Å^{-3})	3.771/−3.893 (e Å^{-3})

chamber. After pumping to between 4 and 5 × 10^{-5} Pa, the sample was transferred to the precooled (−160 °C) manipulator where it was kept until the base vacuum of 4 to 6 × 10^{-7} Pa in the analysis chamber was reached.

The binding energy (BE) scale was referenced to the C 1s line of aliphatic hydrocarbon contamination, set at 285.0 eV. This value was taken from "XPS of Polymers Database".[22] The uncertainty in the BE value's determination was ±0.1 eV, and ±10% rel in atomic ratios. Processing of the spectra was accomplished with Kratos software.

3.6. Luminescence Spectroscopy. Luminescence excitation and emission spectra of the solid compounds were recorded by a Perkin-Elmer LS50B spectrometer using a sample holder developed for powders. Time-resolved spectra and luminescence decay were obtained by laser flash photolysis equipment described elsewhere.[23] The excitation was performed by the third harmonic of the Nd:YAG laser with a 5 ns pulse width.

Results

1. Spectroscopic Studies in Solution. UV and NMR spectroscopy were used to study solutions with a wide range of concentrations ($c_M = 0.0001-1$ M) in order to check the interaction between the coordinative saturated metal complexes, i.e., $[M(CN)_4]^{2-}$ (M = Pt, Pd, Ni) and $Hg(CN)_2$. There was no change in the UV spectrum of $[Pt(CN)_4]^{2-}$ (characteristic bands with absorption maximum at 215, 240, 250, and 280 nm) upon addition of $Hg(CN)_2$ solution. The spectra showed the superposition of the spectra of the starting solutions, and they were unchanged even after a few weeks. These measurements had to be done in relatively dilute samples (0.0001−0.05 M) because of the large molar absorption coefficient ($\epsilon \approx 10^4$ M^{-1} cm^{-1}). However, solutions of $c_{Pt} = c_{Hg} = 1$ M could be measured by NMR. Superposition of the ^{13}C NMR spectra of the $Hg(CN)_2$ and $[Pt(CN)_4]^{2-}$ species could be seen in the spectra with unchanged chemical shift and spin−spin coupling constant values (147.5 ppm and $^1J_{Hg-C} = 3222$ Hz and 128 ppm and $^1J_{Pt-C} = 1032$ Hz, respectively). Neither new ^{13}C NMR signals nor two-bond *Hg*−Pt−C or *Pt*−Hg−C spin−spin coupling constants could be observed. The spectra were similar also when 0.5 M NaCN was added, except for the effect of fast ligand-exchange reaction between $Hg(CN)_2$ and free CN^-, resulting in a time-averaged signal at 154 ppm with no visible coupling between the ^{201}Hg and ^{13}C nuclei. The ^{195}Pt NMR spectrum showed only the signal of $Pt(CN)_4^{2-}$ at −214 ppm. The ^{13}C NMR signal of $Ni(CN)_4^{2-}$ at 138.2 ppm was not changed by the presence of $Hg(CN)_2$, although the ^{201}Hg−^{13}C coupling could not be seen. Only a broad signal was observed, which was attributed to the exchange decoupling. These observations showed clearly the lack of interaction between the square planar $[M(CN)_4]^{2-}$ and $Hg(CN)_2$ complexes in solution.

2. Studies of the Solid Compounds. 2.1. Single-Crystal X-Ray Studies. Slow cooling of a solution with (typically)

(22) *XPS of Polymers Database*; Beamson, G., Briggs, D., Eds.; SurfaceSpectra Ltd.: Manchester, UK, 2000.
(23) Fodor, L.; Horváth, A. *J. Photochem. Photobiol. A* **1998**, *112*, 213−223.

Table 2. Selected Bond Lengths and Angles (Å, deg) of $K_2PtHg(CN)_6 \cdot 2H_2O$ (**1**)[a]

Pt1−Hg1	**3.460(1)**	C1−N1	1.149(11)
C1−Pt1^{i}	1.979(9)	C2−N2	1.159(11)
C2−Pt1^{i}	1.979(9)	C3−N3	1.129(13)
C3−Hg1	2.020(14)	N2−Hg1^{ii}	2.823(12)
K1−O1	2.747(8)	O1−H1O1	0.854(37)
N1−K1	2.863(7)	O1−H2O1	0.846(45)
C1−Pt1−C2^{i}	89.70(34)	N2−C2−Pt1^{i}	177.91(77)
C2^{i}−Pt1−C1^{i}	90.30(34)	Hg1^{ii}−N2−C2	139.43(62)
C3^{iii}−Hg1−C3	180.00(56)	K1−N1−C1	112.12(56)
N2^{iv}−Hg1−C3	93.75(32)	O1^{vi}−K1−O1	77.89(23)
C3−Hg1−N2^{v}	86.25(32)	K1^{vi}−O1−K1	102.11(25)
N3−C3−Hg1	176.90(131)		
N1−C1−Pt1	179.40(79)		

[a] Symmetry codes: (i) $-x, -y, -z$; (ii) $-x, 0.5 + y, -0.5 - z$; (iii) $-x, -1 - y, -z$; (iv) $x, -0.5 - y, 0.5 + z$; (v) $-x, -0.5 + y, -0.5 - z$; (vi) $-1 - x, -1 - y, -1 - z$.

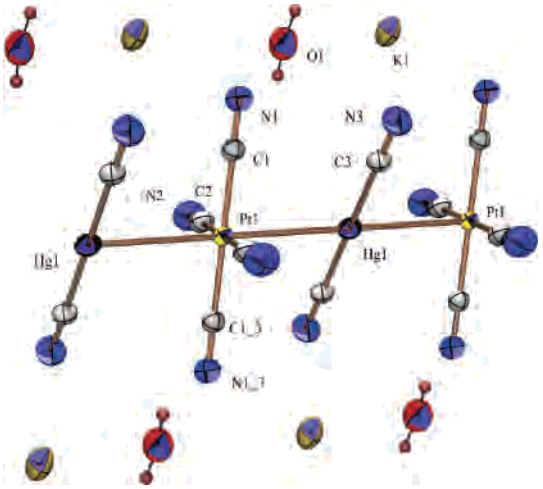

Figure 1. Fraction of the structure of $K_2PtHg(CN)_6 \cdot 2H_2O$ (**1**) at 50% probability level. $d_{Hg-Pt} = 3.46$ Å.

1 M $K_2[Pt(CN)_4]$ and 1 M $Hg(CN)_2$ yielded colorless crystals of $K_2PtHg(CN)_6 \cdot 2H_2O$ (**1**). The molar ratio of K/Pt/Hg was 2:1:1, as measured by scanning electron microscopy, indicated the formation of the adduct described by Strömholm.[24a] A crystal (selected from a sample of the adduct after checking the homogeneity by scanning electron microscopy) was studied by means of the single-crystal X-ray diffraction method, and the structural data are shown in Tables 1 and 2. The fraction of the structure and the view normal to [001] for **1** are shown in Figures 1 and 2. Pd and Ni analogues, $Na_2PdHg(CN)_6 \cdot 2H_2O$ (**2**) and $K_2NiHg(CN)_6 \cdot 2H_2O$ (**3**), were prepared in a similar way and studied by the single-crystal X-ray diffraction method. Selected structural data are shown

(24) (a)The original description of Strömholm[16] was not quite clear as to whether the Hg/Pt molar ratio was 1 or 1.2, i.e., $K_2[Pt(CN)_4]$ or $K_2[Pt(CN)_4] \cdot 3H_2O$ was the weighing form of the Pt compound. In the case of Hg/Pt = 1.2, i.e., at excess of $Hg(CN)_2$, our product was mainly $Hg(CN)_2$(s), but some $K_2PtHg(CN)_6 \cdot 3H_2O$(s) was also formed on the surface of the larger $Hg(CN)_2$ crystals according to pictures obtained by the scanning electron microscope. This kind of inhomogeneity was not observed in the case of Hg/Pt = 1 in the starting solution. (b)Detailed experiments were done on the $[Pd(CN)_4]^{2-}$−Tl(III)−CN^- system in order to find the Pd analogues of the $[(CN)_5Pt-Tl(CN)]_n^{n-}$ family. Using similar conditions as in the case of Pt−Tl compounds, no similar metal−metal-bonded complexes have been detected so far. It might be explained by the different redox potentials, but one can note the larger kinetic lability of the Pd complex compared to $Pt(CN)_4^{2-}$.

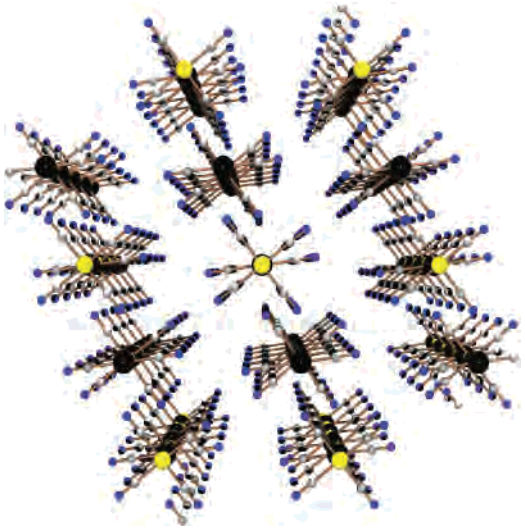

Figure 2. View of $K_2PtHg(CN)_6 \cdot 2H_2O$ (**1**) normal to [001]; K^+ and H_2O are omitted for clarity. Color code: Pt, yellow; Hg, black; N, blue; C, gray.

Table 3. Selected Bond Lengths and Angles (Å, deg) of $Na_2PdHg(CN)_6 \cdot 2H_2O$ (**2**)[a]

Pd1−Hg1	**4.924(37)**	Na1−N3^{v}	2.612(46)
Hg1−C1^{i}	2.038(37)	Na1−Na1^{iv}	3.629(43)
Pd1−C2	1.982(16)	Na1−Na1^{iii}	3.770(4)
Pd1−C2^{ii}	1.982(16)	Na1−Na1^{vi}	3.770(4)
Pd1−C3	1.992(23)	Na1−Na1^{v}	3.780(25)
Pd1−C3^{ii}	1.992(23)	C1−N1	1.130(22)
C1−Hg1−C1^{i}	179.99(27)	N3^{iv}−Na1−Na1^{iii}	43.72(12)
C2−Pd1−C2^{ii}	179.99(26)	N1−Na1−Na1^{iii}	138.33(16)
C2−Pd1−C3	90.64(25)	N3−Na1−Na1^{iii}	92.32(13)
C2^{ii}−Pd1−C3	89.36(25)	N3^{v}−Na1−Na1^{iii}	137.64(14)
C2−Pd1−C3^{ii}	89.36(25)	Na1^{iv}−Na1−Na1^{iii}	61.41(7)
C2^{ii}−Pd1−C3^{ii}	90.64(25)	O1−Na1−Na1^{vi}	99.72(29)
C3−Pd1−C3^{ii}	180.00(24)	O2−Na1−Na1^{vi}	78.34(29)

[a] Symmetry codes: (i) $-x, -y, -z$; (ii) $1 - x, -y, 1 - z$; (iii) $1 + x, y, z$; (iv) $2 - x, 1 - y, 1 - z$; (v) $1 - x, 1 - y, 1 - z$; (vi) $-1 + x, y, z$.

Table 4. Selected Geometric Parameters (Å, deg) of $K_2NiHg(CN)_6 \cdot 2H_2O$ (**3**)[a]

Ni1−Hg1	**4.613(1)**	C4−N4^{iv}	1.140(19)
Hg1−N3^{i}	2.710(13)	O1W−K1^{i}	2.733(13)
Ni1−C4	1.868(13)	H1O−O1W	0.953(47)
Ni1−C3^{ii}	1.861(14)	H2O−O1W	0.944(125)
Hg1−C1	2.001(16)	K1−O1W	2.782(15)
Hg1−K1^{iii}	5.390(33)	Ni1−Ni1^{iii}	4.024(1)
C1−N1	1.220(20)	Hg1−Hg1^{iii}	4.024(1)
N3−C3	1.150(20)		
C3−Ni1−C4	90.06(58)	K1^{i}−O1W−K1	93.74(50)
C4^{ii}−Ni1−C3	89.94(58)	H1O−O1W−H2O	89.31(1219)
C1−Hg1−C1^{v}	169.41(62)	N3^{i}−Hg1−N3^{vi}	95.20(37)
Hg1^{iii}−N3−C3	160.44(116)	N3−C3−Ni1	177.33(136)
N3^{i}−Hg1−C1	92.85(56)	N4^{iv}−C4−Ni1^{ii}	179.43(132)
N3^{vi}−Hg1−C1	94.29(56)		

[a] Symmetry codes: (i) $x, 1 + y, z$; (ii) $2 - x, -y, 1 - z$; (iii) $x, -1 + y, z$; (iv) $x, -y, 0.5 + z$; (v) $2 - x, y, 0.5 - z$; (vi) $2 - x, 1 + y, 0.5 - z$.

in Tables 1, 3 and 4. Figures 3 and 4 present the packing diagram of **2** and an Ortep view of **3**, respectively.

2.2 Raman Spectra of Selected Solids. Raman spectra of the solids **1** and **3** were recorded together with the spectra of the starting materials, $K_2[Pt(CN)_4] \cdot 3H_2O$, $K_2[Ni(CN)_4] \cdot 3H_2O$, and $Hg(CN)_2$. A spectrum of compound **1** is shown in Figure 5. Frequencies of the bands are collected in Tables 5 and 6.

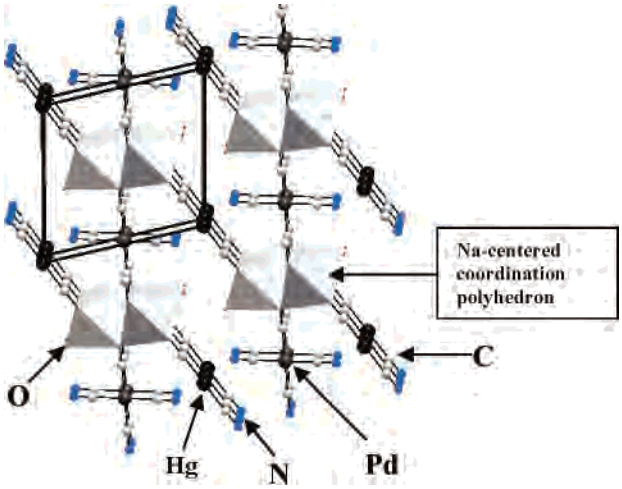

Figure 3. Packing diagram of $Na_2PdHg(CN)_6 \cdot 2\ H_2O$ (**2**). $d_{Hg-Pd} = 4.92$ Å.

Figure 4. Ortep view of $K_2NiHg(CN)_6 \cdot 2H_2O$ (**3**) at 50% probability level. $d_{Hg-Ni} = 4.61$ Å.

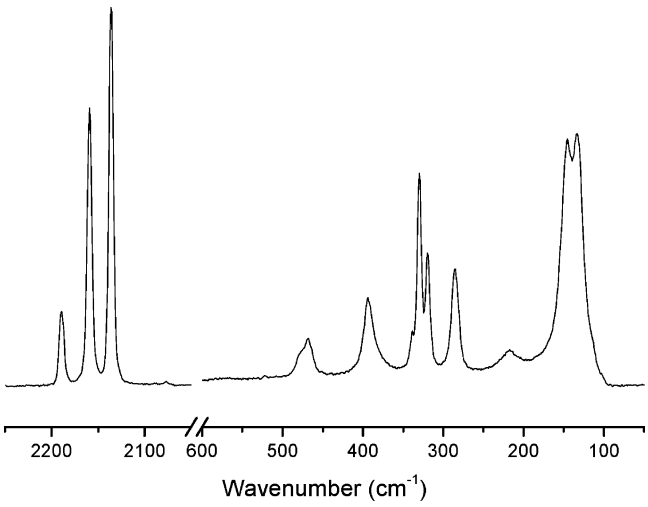

Figure 5. Raman spectrum of the $K_2PtHg(CN)_6 \cdot 2H_2O$ (**1**) compound.

2.3. XPS Measurements of the Solids. XPS data were collected for **1**, **2**, and **3** together with the data of the parent cyano complexes, $K_2[Pt(CN)_4] \cdot 3H_2O$, $Na_2[Pd(CN)_4] \cdot 3H_2O$, $K_2[Ni(CN)_4] \cdot 3H_2O$, and $Hg(CN)_2 \cdot 2H_2O$. The data for $K_2[Pt(CN)_6] \cdot 3H_2O$ were also measured in order to compare the BEs of Pt(II) and Pt(IV). Data are collected in Tables 7−9.

2.4. Luminescence Spectroscopy. Excitation spectra of $K_2[Pt(CN)_4] \cdot 3H_2O$ and $K_2PtHg(CN)_6 \cdot 2H_2O$ with emission spectra of complexes obtained by different excitation wavelengths ($\lambda_{exc} = 244$ nm and $\lambda_{exc} = 384$ nm) can be seen in Figure 6. The low energy range of excitation spectra and

Table 5. Raman Frequencies (cm^{-1}) of $K_2PtHg(CN)_6 \cdot 2H_2O$ (**1**) and the Parent Compounds $K_2[Pt(CN)_4] \cdot 3H_2O$ and $Hg(CN)_2$

$K_2PtHg(CN)_6 \cdot 2H_2O$	$K_2[Pt(CN)_4] \cdot 3H_2O$[a]	$Hg(CN)_2$[b]
2189		2196/ ν_s(CN)
2159	2165/ν_s(CN)	
2136	2144/ν_a(CN)	
477	473/ν_a(PtC)	
468	466/ν_s(PtC)	431/ν_s(HgC)
394		396/ δ(HgCN)
330		341
319	322/δ(PtCN)	
285		283/δ(CHgC)
218		
	172/δ(CPtC)	
146	148	
134	131	131
		121

[a] Assignment of the bands according to Kubas et al.[30] [b] Assignment of the bands according to Jones et al.[31]

Table 6. Raman Frequencies (cm^{-1}) of $K_2NiHg(CN)_6 \cdot 2H_2O$ (**3**) and the Parent Compounds $K_2[Ni(CN)_4] \cdot H_2O$ and $Hg(CN)_2$

$K_2NiHg(CN)_6 \cdot 2H_2O$	$K_2[Ni(CN)_4] \cdot H_2O$[a]	$Hg(CN)_2$[b]
2188		2196/ ν_s(CN)
2136	2141/ν_s(CN)	
2124	2133/ν_a(CN)	
424	415/ν_a(NiC)	
411	405/ν_s(NiC)	431/ν_s(HgC)
392		396/ δ(HgCN)
334		341
301	302/δ(NiCN)	
285		283/δ(CHgC)
	180/δ(CNiC)	
150	148	
		131
	123	121

[a] Assignment of the bands according to Kubas et al.[30] [b] Assignment of the bands according to Jones et al.[31]

Table 7. Binding Energy Values (eV) Measured by XPS for $K_2PtHg(CN)_6 \cdot 2H_2O$ (**1**) and Its Components, $K_2[Pt(CN)_4] \cdot 3H_2O$ and $Hg(CN)_2$

line	$K_2PtHg(CN)_6 \cdot 2H_2O$ BE, eV	$K_2[Pt(CN)_4] \cdot 3H_2O$ BE, eV	$K_2[Pt(CN)_6]$ BE, eV	$Hg(CN)_2$ BE, eV	
C 1s	**285.0**	**285.0**	**285.0**	**285.0**	**C**−(C,H)
	285.8	285.8	286.3		Pt−**C**N
	286.6			286.1	Hg−**C**N
N 1s	398.8	398.7	398.3		Pt(II)-C**N**
	399.7		399.4	399.4	Hg−C**N**, Pt(IV)-C**N**
	400.9	399.7	400.7		Pt−**N**C (tentative)
K $2p_{3/2}$	293.7	293.5	293.3		
Pt $4f_{7/2}$	74.0	73.9	74.0		**Pt**(II)-CN
		75.2			**Pt**−NC (tentative)
			77.2		**Pt**(IV)-CN
Hg $4f_{7/2}$	102.4			102.4	**Hg**−CN

the emission spectra of $K_2[Pt(CN)_4] \cdot 3H_2O$ and **1** complexes are very similar, indicating the same lowest-energy chromophore and luminophore of for the two samples. The excitation and emission spectra of $Hg(CN)_2$ have been also recorded. The intensity of these spectra is significantly lower than that of complex **1**. The emission band shows a peak at 390 nm, while the maximum in the excitation spectrum appears at 240 nm.

Figure 7 shows the luminescence decays initiated by excitation of crystalline $K_2[Pt(CN)_4] \cdot 3H_2O$ and **1** complexes using a laser pulse ($\lambda_{exc} = 355$ nm). Both curves show double exponential decay, the short-lived emitting states have $\tau_{1Pt} = 80 \pm 20$ ns and $\tau_{1Pt-Hg} < 10$ ns, while the longer-lived excited states have $\tau_{2Pt} = 550 \pm 30$ ns and $\tau_{2Pt-Hg} = 290 \pm$

Table 8. Binding Energy Values (eV) Measured by XPS for $Na_2PdHg(CN)_6 \cdot 2H_2O$ (**2**) and Its Component, $Na_2[Pd(CN)_4] \cdot 3H_2O$

line	$Na_2PdHg(CN)_6 \cdot 2H_2O$ BE, eV	$Na_2[Pd(CN)_4] \cdot 3H_2O$ BE, eV	$Hg(CN)_2$ BE, eV	
C 1s	**285.0**	**285.0**	**285.0**	**C**−(C,H)
	285.8	285.8		Pd−**C**N
	286.5		286.1	Hg−**C**N
N 1s	398.8	398.9		Pd−C**N**
	399.7		399.4	Hg−C**N**
		399.8		Pd−**N**C (tentative)
	400.6			Hg−**N**C (tentative)
Na 1s	1071.6	1071.3		
		1073.0		
Pd $3d_{5/2}$	339.3	339.4		**Pd**−CN
Hg $4f_{7/2}$	102.4		102.4	**Hg**−CN

Table 9. Binding Energy Values (eV) Measured by XPS for $K_2NiHg(CN)_6 \cdot 2H_2O$ (**3**) and Its Component, $K_2[Ni(CN)_4] \cdot 3H_2O$

line	$K_2NiHg(CN)_6 \cdot 2H_2O$ BE, eV	$K_2[Ni(CN)_4] \cdot 3H_2O$ BE, eV	$Hg(CN)_2$ BE, eV	
C 1s	**285.0**	**285.0**	**285.0**	**C**−(C,H)
	285.8	285.9		Ni−**C**N
	286.8		286.1	Hg−**C**N
N 1s	399.0	399.0		Ni−C**N**
	400.1	399.9	399.4	Hg−C**N**
K $2p_{3/2}$	294.0	293.5		
Ni $2p_{3/2}$	856.2	856.1		**Ni**−CN
Hg $4f_{7/2}$	102.8		102.4	**Hg**−CN

15 ns lifetime values for $K_2[Pt(CN)_4] \cdot 3H_2O$ and **1**, respectively. Comparing the longer lifetime measured for $K_2[Pt(CN)_4] \cdot 3H_2O$ crystals with that of the phosphorescencent $[Pt(CN)_4]^{2-}$ oligomer reported by Schindler et al.[14] (525−560 ns), the radiative decay characterized by a lifetime of 550 ± 30 ns can be assigned to a spin-forbidden transition. On the other hand, the short-lived luminescence (80 ± 20 ns) of the $K_2[Pt(CN)_4] \cdot 3H_2O$ crystals is expected to originate from a singlet excited state.

Discussion

1. Solution Studies. All experimental findings in solution by UV−vis and NMR spectroscopy have clearly shown the lack of interaction between $Hg(CN)_2$ and the square planar d^8 transition metal complexes, $[M(CN)_4]^{2-}$ (M = Pt, Pd, or Ni). Keeping in mind the outstanding stability of the $[(CN)_5Pt-Tl(CN)_n]^{n-}$ complexes,[7] it is somewhat surprising, especially in the case of the Pt(II)−Hg(II) system, because Hg(II) and Tl(III) are isoelectronic and their cyano complexes behave quite similarly. DFT calculations for the $[(CN)_5Pt-Tl(CN)]^-$ have shown the role of the (N)C−Pt−Tl linear, three-atom entity.[10] The relative oxidation state of the metal centers[4,5] indicates electron transfer from Pt to Tl, or in other words, Tl(III) can partially oxidize Pt(II). Although the formal redox potential values valid for our experimental conditions (having cyanide ligands present) are not available, it is quite rational that Hg(II) is a weaker oxidant than Tl(III). It might indicate the important role of the redox potential in the formation of metal−metal-bonded cyano complexes.[24b] Realizing that $Hg(CN)_2$ does not react with $Pt(CN)_4^{2-}$ in solution, we have not expected strong interactions between $Hg(CN)_2$ and the $Pd(CN)_4^{2-}$ and $Ni(CN)_4^{2-}$ complexes and our interest has been focused on the solid adducts, see below.

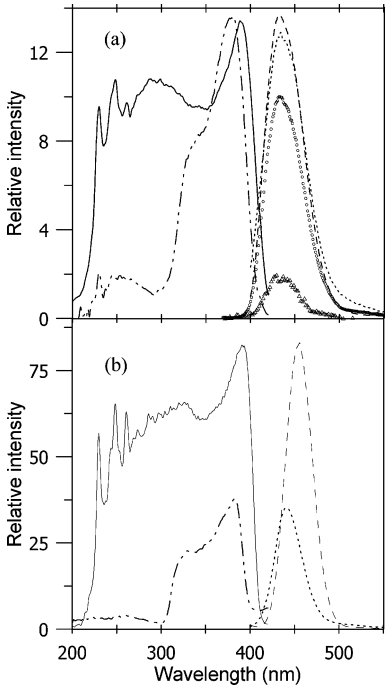

Figure 6. Comparison of excitation and emission spectra of $K_2[Pt(CN)_4] \cdot 3H_2O$ (Pt) and $K_2PtHg(CN)_6 \cdot 2H_2O$ (**1**) crystals detected at 298 (a) and at 77 K (b), respectively: excitation spectra of Pt (continuous line) and those of (**1**) (− · ·), emission spectra of Pt obtained by excitation at λ_{exc}=384 nm (− − −) and at λ_{exc} = 244 nm (○) and those of **1** at λ_{exc}=384 nm (· · ·) and at λ_{exc} = 244 nm (△).

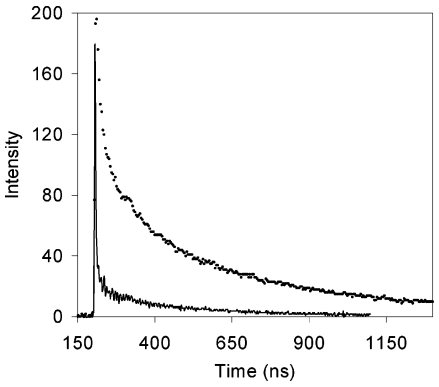

Figure 7. Luminescence decay of $K_2[Pt(CN)_4] \cdot 3H_2O$ (· · ·) and $K_2PtHg(CN)_6 \cdot 2H_2O$ (**1**) (—) after the excitation of 355 nm laser pulse; $\tau_{1(Pt)} = 80 \pm 20$ ns, $\tau_{2(Pt)} = 550 \pm 30$ ns, $\tau_{1(Pt-Hg)} < 10$ ns, $\tau_{2(Pt-Hg)} = 290 \pm 15$ ns.

2. Studies of the Solid Compounds. 2.1. X-Ray Structures. X-ray data confirm that the stoichiometry of the single crystal **1** is the same as the formula published by Strömholm.[16] A fraction of the structure is shown in Figure 1. The Pt−Hg distance at 3.460 Å is much longer than the Pt−Tl distance in the Pt−Tl-bonded compounds (d_{Tl-Pt} = 2.60 Å). This is in accordance with the experimental results in solution, i.e., there is no chemical bond between the two heavy atoms. However, d_{Hg-Pt} = 3.460 Å is much shorter than the distance between the Hg atoms in $Hg(CN)_2$(s), d_{Hg-Hg} = 4.501 and 4.989 Å,[25] and it is also shorter than d_{Pt-Pt} = 3.48 Å in $K_2[Pt(CN)_4] \cdot 3H_2O$,[26] in which the

(25) Seccombe, R. C.; Kennard, C. H. L. *J. Organomet. Chem.* **1969**, *18*, 243−247.
(26) Washecheck, D. M.; Peterson, S.; Reis, A. H., Jr.; Williams, J. M. *Inorg. Chem.* **1976**, *15*, 74−78.

$[Pt(CN)_4]^{2-}$ units are rotated by 45°, resulting in optimal 'stacking' interactions. In contrast, in **1**, the $Pt(CN)_4^{2-}$ units (having almost 180° Pt−C−N angles) are eclipsed and $Hg(CN)_2$ rotated by 30° is located in between. This arrangement might be less favorable for 'stacking'; therefore, other interaction(s) could be responsible for the relatively short d_{Hg-Pt}. There is a very weak H bond in the lattice between the O atom of the lattice water molecules and one of the N atoms of the Pt-bonded cyanides: $d_{O-N} = 3.068(13)$ Å (a typical distance for strong O−H···N is 2.68−2.79 Å).[27] This interaction, together with some Pt−Hg attraction, may explain the relatively short Pt−Hg distance. The issue 'if this metallophilic interaction can be detected by Raman or XPS method' will be discussed below. The structure in Figure 1 and the formula resemble the structure and stoichiometry of $Cs_2[Au(I)Cl_2][Au(III)Cl_4]$. In fact, the Au(I)−Au(III) entity is isoelectronic with the Pt(II)−Hg(II) entity. However, the linear $[Au(I)Cl_2]^-$ anions connect the square planar $[Au(III)Cl_4]^-$ anions through Cl bridges; therefore, the metal atoms are quite far from each other in the formally Au(II)−chloride compound.[27]

A different view of the structure of **1** can be seen in Figure 2. A closer look clearly indicates that the lattice consist of infinite $(-Pt-Hg-)_n$ 'one-dimensional wires' without bridging cyanides. The distance between the closest wires is 5.607 Å. In a plane perpendicular to the $(-Pt-Hg-)_n$ chain, Pt and Hg atoms alternate. The weakly hydrated K^+ counterions are located between the polymer chains; the water molecules stabilize the lattice by H bonds, see above. The strictly linear chain, characteristic for one-dimensional conductors, is similar to the partially oxidized Pt(II)−cyano complexes, e.g., $K_{1.75}Pt(CN)_4 \cdot 1.5H_2O$. The renaissance of chain compounds based on transition metal backbone has recently been reviewed.[28] Conductivity measurements of **1** are in progress.

The structures determined for **2** and **3** are not similar to the structure of **1**. The unit cell of **2** can be seen in Figure 3. The cell consists of Na^+ ions, which are coordinated by five cyanide-N atoms and one water molecule. The coordination polyhedron is an octahedron, which is only slightly distorted. The Na-centered octahedra share edges which each other, yielding double chains. These chains are bridged by Pd^{2+} ions, each of which carries another two C-bonded cyanide groups, and by Hg^{2+} ions yielding a three-dimensional network. The Hg^{2+} ions are weakly coordinated by four N atoms of surrounding CN^- groups ($d_{Hg-N} \approx 2.8$ Å). The coordination geometry of Pd is a slightly distorted square plane. The Hg(II) ions are coordinated by two cyanide groups in a linear fashion. Taking into account the four additional cyanide groups, the polyhedron is a very distorted octahedron. Both the linear $Hg(CN)_2$ units and square planar $[Pd(CN)_4]^{2-}$ entities are eclipsed. The structure can be considered as a double salt; the lack of heterometallophilic interaction between the remote Hg(II) and Pd(II) atoms, $d_{Hg-Pd} = 4.92$ Å seems obvious. This is in agreement with the solution studies.

As expected, the structure of **3** shown in Figure 4 is also dominated by the alternately located layers of $Hg(CN)_2$ and $[Ni(CN)_4]^{2-}$. The value of $d_{Hg-Ni} = 4.61$ Å precludes the possibility of heterometallic interaction.

2.2. Raman Spectroscopy. Raman spectroscopy is usually very useful for identification of vibrations attributed to symmetrical metal−metal stretches.[29,30] Thus, for example, strong bands, indicative of nonbuttressed Pt−Tl and Pt−Pt metal−metal bonds, have been observed in a series of related compounds $[(NC)_5Pt-Tl(CN)_n]^{n-}$ and a species $[(NC)_5Pt-Pt(CN)_5]^{4-}$ at about 160 and 145 cm^{-1}, respectively, both in solution and in the solid state. The corresponding bond lengths are 2.60−2.64 and 2.73 Å, respectively.[4,31] Taking into account both the lack of bonding between the metallic centers for the Pt(Pd,Ni)−Hg systems in solution and long intermetallic distances in the solids (vide supra), one can hardly expect the M−Hg stretching vibration to appear in Raman spectra of the solid compounds (**1**−**3**). However, comparison of vibrational spectra of the heterometallic and parent cyanide compounds is of obvious interest. Because of high sensitivity of frequencies of molecular vibrations to even small changes both in structure and in oxidation states,[30] vibrational spectroscopy can provide valuable information on structural and bonding features in the studied heterometallic systems.

Vibrational spectra of cyano compounds of $[M(CN)_4]^{2-}$ (M = Pt, Pd, Ni) and $Hg(CN)_2$ were thoroughly studied by Jones et al.[32,33] Raman frequencies of the vibrational bands for the compounds of $[M(CN)_4]^{2-}$ and $Hg(CN)_2$, presented in Tables 5 and 6, are in good agreement with the data in the cited papers. Figure 5 and Tables 5 and 6 clearly show that, in the case of both compounds **1** and **3**, the majority of the bands found in the spectra of the parent compounds can be recognized in the spectra of the adducts. Both $[M(CN)_4]^{2-}$ and $Hg(CN)_2$ behave therefore as discrete entities, preserving their original symmetry and structure in the heterometallic compounds. Comparing the frequencies of the bands in the adducts and in the starting compounds reveals, however, that there are small but notable shifts in the band positions for the most indicative C−N and M−C stretching vibrations. The frequency of the M−C stretch in the $[M(CN)_4]^{2-}$ unit is increased in the heterometallic complex compared to the parent compounds, indicating some strengthening in the metal−carbon bonding. This is accompanied by an expected weakening (decrease of the wavenumber) for the corresponding C−N bonds. A similar trend, namely shift of $\nu_s(CN)$ to lower wavenumbers, is observed for the $Hg(CN)_2$ entity as well (cf. Tables 5 and 6).

A number of bands also appear in the low-frequency region (>150 cm^{-1}) of the Raman spectra of the compounds.

(27) Greenwood, N. N.; Earnshaw, A. *Chemistry of the Elements* 2nd ed.; Butterworth-Heinemann: Oxford, 1997; p 60; p 1189.
(28) Durham, K. R.; Bera, J. K. *Angew. Chem., Int. Ed.* **2002**, 4453.
(29) Cotton, F. A.; Walton, R. A. *Multiple Bonds Between Metal Atoms*, 2nd ed.; Clarendon Press: Oxford, 1993.
(30) Nakamoto, K. *Infrared and Raman Spectra of Inorganic and Coordination Compounds*, 5th ed.; Wiley-Interscience: New York, 1997.
(31) Jalilehvand, F.; Maliarik, M.; Mink, J.; Sandström, M.; Ilyukhin, A.; Glaser, J. *J. Phys. Chem.* **2002**, *104*, 3501−3516.
(32) Kubas, G. J.; Jones, L. H. *Inorg. Chem.* **1974**, *13*, 2816−2819.
(33) Jones, L. H. *Spectrochim. Acta* **1963**, *19*, 1675.
(34) Viswanath, A. K.; Patterson, H. H. *Chem. Phys. Lett.* **1981**, *82*, 25−28.

These bands cannot be assigned to the metal−metal stretching vibrations since this would result in unreasonably high (for the studied heterometallic systems) force constants of the M−M′ bond.[4] For example, the force constant calculated for the Pt−Pt bond in the $[(NC)_5Pt-Pt(CN)_5]^{4-}$ complex, which exhibits a strong Raman band at 145 cm^{-1} (ν_s(Pt−Pt)) in solution and has the metal−metal bond length of 2.73 Å, is 123.8 N m^{-1}. One can see that the bands in this region are also found in the spectra of the starting compounds. These bands probably arise from mixed modes involving bending CMC vibrations and/or lattice vibrations.

2.3. XPS Measurements. A three-dimensional X-ray structure gives the most valuable data, but it gives only limited information about the oxidation state of the metal centers. Although the metal−metal distances measured in **1** and especially in **2** and **3** preclude any significant bonding, we have made XPS measurements in order to correlate the structure and the BEs of the electrons at the metal centers. XPS could also be used as an analytical tool to check the stoichiometry of the adducts usually prepared at a very small scale.

BE values are summarized in Tables 7−9. The BE of Pt $4f_{7/2}$ electrons is 74.0 eV for the adduct **1** and 73.9 eV in $K_2[Pt(CN)_4]\cdot 3H_2O$, while the BE of Hg $4f_{7/2}$ electrons is 102.4 eV for both **1** and $Hg(CN)_2$. All these values are equal or do not differ significantly; therefore, no change in the 'relative oxidation state' of the metal centers can be concluded. This is in contrast to the experimental findings for $(CN)_5PtTl(s)$ having a strong Pt−Tl bond.[5] As expected, the BE values of the Ni $2p_{3/2}$ electrons in **3** and in $K_2[Ni(CN)_4]\cdot 3H_2O$ are not significantly different, 856.2 and 856.1 eV, respectively. A similar situation has been observed for Pd $3d_{5/2}$, 339.3 eV in **2** and 339.4 in $Na_2[Pd(CN)_4]\cdot 3H_2O$. The BE of Hg $4f_{7/2}$ electrons is 102.4 eV for **2**, being the same as the value of 102.4 eV in $Hg(CN)_2$, as it should be if the counter metal centers (Ni and Pd) have not been changed. In the case of Ni, it looks like the $Hg(CN)_2$ fragment shows not only an increase in C 1s and N 1s BEs but also in the Hg $4f_{7/2}$ one. This increase is larger than in the case of Pt and Pd, but it can still be attributed to the uncertainty of the measurements.

2.4. Luminescence Measurements. Luminescence spectra of $K_2[Pt(CN)_4]\cdot 3H_2O$ and $K_2[PtHg(CN)_6]\cdot 2H_2O$ are shown in Figure 6. The characteristics of the spectra can be compared to the results of the detailed emission studies of $Ba[Pt(CN)_4]$[15] and of various other crystalline $M_n[Pt(CN)_4]\cdot xH_2O$ complexes (M = K and Na, K and Li, Mg, Sr, $n = 1$ or 2 for alkaline or alkaline earth cations, respectively). Experiments using external pressure on the crystals (1−28 kbar) have shown that the energy of the emitted light is linearly dependent on the Pt−Pt distance.[12,13] Considering the data of ref 13, one can estimate an emission maximum for a microcrystalline-disordered sample of $K_2[Pt(CN)_4]\cdot 3H_2O$ to be between 420 and 440 nm and the appearance of the emission at somewhat longer wavelengths for **1**, in good agreement with the observed emission on the spectra in Figure 6. On the other hand, the spectra of heteronuclear species show a slightly more pronounced Stokes shift than that of $K_2[Pt(CN)_4]\cdot 3H_2O$ at 298 K. It should be noted that the Stokes shift of $K_2[Pt(CN)_4]\cdot 3H_2O$ is more pronounced at 77 K (3500 cm^{-1}) than at 298 K (2600 cm^{-1}) due to the significant red shift of the emission spectrum with decreasing temperature, as it has also been observed by Gliemann et al.[12] However, the Stokes shifts for the spectra of the Pt−Hg complex obtained at ambient temperature (3400 cm^{-1}) and at 77 K (3380 cm^{-1}) are the same within experimental error. Moreover, the excitation spectrum of the parent $K_2[Pt(CN)_4]\cdot 3H_2O$ compound has a more intense broad band between 230 and 340 nm compared to the one of the heteronuclear complex in this range. This experimental finding indicates the formation of luminescent excited states with a relatively high efficiency in crystalline $K_2[Pt(CN)_4]\cdot 3H_2O$. Figure 7 shows the luminescence decays initiated by excitation of the crystalline $K_2[Pt(CN)_4]\cdot 3H_2O$ and **1** compounds using laser pulse (λ_{exc}=355 nm). The very rapid decay of the short-lived emitting state ($\tau_{1Pt-Hg} < 10$ ns vs $\tau_{1Pt} = 80 \pm 20$ ns), as well as the shortening of the lifetime for the longer-lived excited state (from τ_{2Pt}=550±30 ns to $\tau_{2Pt-Hg} = 290 \pm 15$ ns) in the case of **1** due to the incorporation of $Hg(CN)_2$ into the columnar structure of the pure $K_2[Pt(CN)_4]\cdot 3H_2O$, can be explained by a quenching effect of $Hg(CN)_2$ units. In principle, the quenching may occur by means of either energy or electron transfer. Luminescence study on $Ba[(Pt,Ni)(CN)_4]\cdot nH_2O$ crystals has shown a characteristic change of the luminescence spectra with temperature between 24 and 250 K.[34] The narrow luminescence peak (observed at 498 nm and assigned as a fluorescence of an excited-state delocalized over several Pt and Ni centers along the one-dimensional chain) has been decreased in intensity with an increase of temperature, while a new broad emission peak at 560 nm emerged over 125 K and became pronounced with further increase in temperature. The latter has been assigned to a phosphorescence from clusters of $[Pt(CN)_4]^{2-}$ due to energy transfer from the Pt−Ni delocalized excited state. It has also been demonstrated by comparison of $\Delta\nu_{1/2}$ values of the fluorescence band of $Ba[(Pt,Ni)(CN)_4]$ (~900 cm^{-1}) and $Ba[Pt(CN)_4]$ (1340 cm^{-1}) crystals that the delocalization in a pure Pt complex is more pronounced compared to the $Ba[(Pt,Ni)(CN)_4]$ compound. We observe a significantly broader band in the luminescence spectrum of $K_2PtHg(CN)_6\cdot 2H_2O$ than in $K_2[Pt(CN)_4]\cdot 3H_2O$ at both 77 and 298 K, in contrast to the observation for the fluorescence of $Ba[(Pt,Ni)(CN)_4]$ and $Ba[Pt(CN)_4]$ complexes, respectively. Moreover, the feature of the emission spectra of $K_2Pt(CN)_4\cdot 3H_2O$ and $K_2PtHg(CN)_6\cdot 2H_2O$ complexes do not show significant changes between 77 K (Pt = 1720 cm^{-1}, Pt−Hg = 1830 cm^{-1}) and 298 K (Pt = 2610 cm^{-1}, Pt−Hg = 2890 cm^{-1}, see Figure 6). Hence, it might allow us to explain the quenching by an electron transfer in the case of the $K_2PtHg(CN)_6\cdot 2H_2O$ compound. In other words, some electron transfer can be observed between the heterometallic centers in the exited state of **1** by measuring luminescence decay, although all the other spectroscopic methods used ruled out a similar process in the ground state. Further study is needed to explore this phenomenon.

Conclusions

An interaction between $Hg(CN)_2$ and square planar $[M^{II}(CN)_4]^{2-}$ transition metal cyanides (M = Pt, Pd, or Ni, with d^8 electron shell) does not result in a metal−metal bond formation in solution in contrast to the isoelectronic $[Pt^{II}(CN)_4]^{2-}-Tl^{III}(CN)_n^{+3-n}$ system, revealing a strong and not supported Pt−Tl bond. However, well-defined adducts can be prepared and characterized in the solid phase by means of single-crystal X-ray diffraction. The structure of **1** consists of one-dimensional −Pt−Hg−Pt−Hg− wires. No CN^- bridges were observed between the heterometallic centers. The wire is strictly linear, and the Pt(II) and Hg(II) centers alternate; $d_{Hg-Pt} = 3.460$ Å is relatively short. Time-resolved luminescence spectra indicate that $Hg(CN)_2$ units incorporated into the structure act as electron traps and shorten the lifetimes of both the short-lived and the longer-lived exited states in **1** compared to $K_2[Pt(CN)_4]\cdot 3H_2O$. The quenching mechanism might be an electron-transfer instead of an energy-transfer process.

The other adducts, **2** and **3**, do not show similarity with the structure of **1**. The structures can be considered as double salts, the lack of heterometallophilic interaction between both remote Hg(II) and Pd(II) atoms, $d_{Hg-Pd} = 4.92$ Å, and Hg(II) and Ni(II) atoms, $d_{Hg-Ni} = 4.61$ Å, seems to be obvious. Electron BE values of the metallic centers measured by XPS show that no electron transfer between the metal ions occurs in the three adducts.

Acknowledgment. The project was financed by Hungarian OTKA T038296 and T043365. A.C.B. is grateful to the Hungarian Ministry of Education for I. Széchenyi Fellowship, while I.T. would like to thank the Wenner-Gren Stiftelserna for a Fellowship. The authors also thank Pál Benyovszki for some preliminary experiments, Professor Attila Horváth for valuable discussions on the photophysics of **1**, and Dr. David Lawrence (Linköping University) for linguistic correction of this manuscript.

Supporting Information Available: Crystallographic data in txt format. This material is available free of charge via the Internet at http://pubs.acs.org.

IC050352C